

## 2-3-7 Ionospheric Dynamo Process

JIN Hidekatsu

Ionospheric electron density varies on various temporal and spatial scales. Because electron density variations affect radio waves reflecting at and penetrating in the ionosphere, their prediction is an important issue for space weather forecast. Some of the ionospheric day-to-day variations are considered to originate in the lower atmospheric activities. Ionospheric dynamo plays an important role in converting from atmospheric waves into the variations in electric field and current. This paper describes the basic theory of ionospheric dynamo, and the generations of global ionospheric current system and electric field distribution which leads to ionospheric density variations. We also introduce our electrodynamics model which represents ionospheric dynamo process. This model is a part of a whole atmosphere-ionosphere coupled model, which is expected to reproduce ionospheric day-to-day variations.

### **Keywords**

Ionospheric dynamo, Space weather, Ionosphere, Atmosphere, Simulation

### **1 Introduction: daily changes in the ionosphere and the ionospheric dynamo**

The ionosphere over Japan, particularly in its southern regions, shows significant changes on a daily basis. For example, Fig. 1 shows daily changes in the total electron content (TEC) over Okinawa as observed over an 80-day period from the beginning of 2006. The middle and bottom panels in Fig. 1 show changes during the daytime (i.e., average from 11:00 to 15:00 LT), and changes around sunset (i.e., average from 17:00 to 21:00LT), respectively. The top panel shows the Kp index that indicates the degree of geomagnetic turbulence. The Kp index during these periods was generally below 3, indicating geomagnetically quiet. The Kp index occasionally fluctuates between 3 and about 5, but the figure apparently suggests that this fluctuation does not correlate with changes in TEC. That is, even though there are no effects from the magnetosphere, significant daily changes occur in the ionosphere at such low latitudes. In terms of

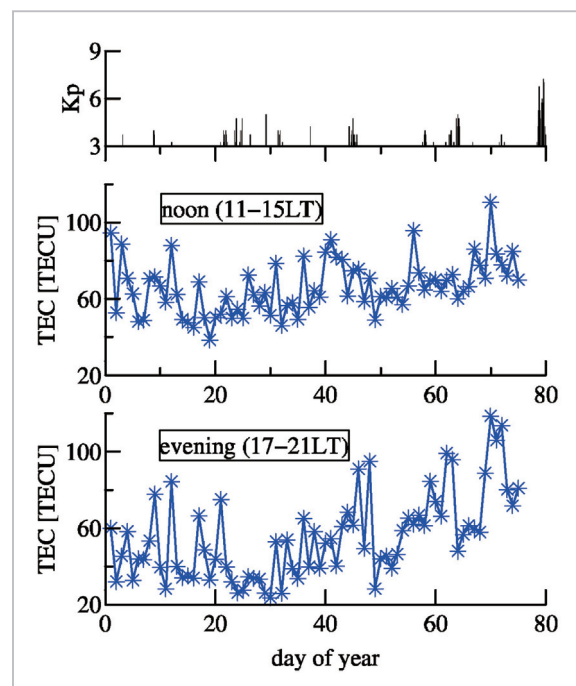


**Fig. 1** Daily changes in the total electron content over southern part of Japan

The Kp index during an 80-day period from the beginning of 2006 (top panel) and changes in the total electron content in the space over Okinawa (middle panel: average from 11:00 to 15:00LT during the daytime; bottom panel: average from 17:00 to 21:00LT around sunset)

its effects on our society, the TEC is a quantity directly linked to radio propagation delay between the ground surface and artificial satellites, and therefore daily changes in TEC can give serious impacts on the use of satellite positioning applications.

These daily changes in the ionosphere over southern Japan are related to the development of “equatorial ionization anomaly (EIA)” to mid-latitudes. The EIA refers to a structure that the largest density region is not located at the equator where the solar radiation flux becomes largest but is separated to the south and north portions across the magnetic equator as shown in Fig. 2. In the formation of the EIA, electric field generated by dynamo process (described later) plays a key role. When the electric field acts on ionospheric plasma, the electric field drift in the direction orthogonal to the magnetic field lines of the earth (poleward/ upward due to eastward electric field) and diffusion toward the poles/downward along the magnetic field lines will generate a distribution of electron densities as shown in Fig. 2. Thus, the dynamo electric field affects the latitudinal spread of

EIA. Southern part of Japan is located on the high-latitude side of EIA, so that the F region electron density during the daytime depends on the degree to which EIA spreads. In other words, changing electric field due to dynamo process is one of major factors behind daily changes in electron density at low to mid latitudes.

This paper presents the ionospheric dynamo that is closely related to changes in the ionosphere at low to mid latitudes. Study of the ionospheric dynamo has a long history. It initiated mainly during the 1950s on a mechanism that connects the ionospheric current system and neutral atmospheric dynamics (e.g., tides, other atmospheric waves) as estimated based on observations of geomagnetic field variation on the ground. For the detailed historical review, see Reference [1] and other materials. In recent years, the importance of ionospheric dynamo has been further recognized from several aspects. One aspect is related to the recent advances in the observation technique, i.e., global remote sensing from satellites and GPS receiver network, these have enabled us to observe broader ionospheric distribution. This resulted in the new discovery of an ionospheric longitudinal structure considered to originate in the lower atmosphere (see Reference [2] in his feature edition). The ionospheric dynamo presumably plays an important role in the linkage between the lower atmosphere and ionosphere. Another aspect is due to advances in the numerical technique, that is, global-scale simulation models that integrate different vertical regions have become possible. The electrodynamics model that treats the ionospheric dynamo is an important component that connects an atmospheric model with an ionospheric model. Advances made in regionally integrated models have allowed researchers to address such challenges as the origin of daily changes in the ionosphere, and the models are expected to be used in future numerical prediction of the upper atmospheric variations. This paper is organized as follows: Chapter 2 briefly describes the basic theory of the ionospheric

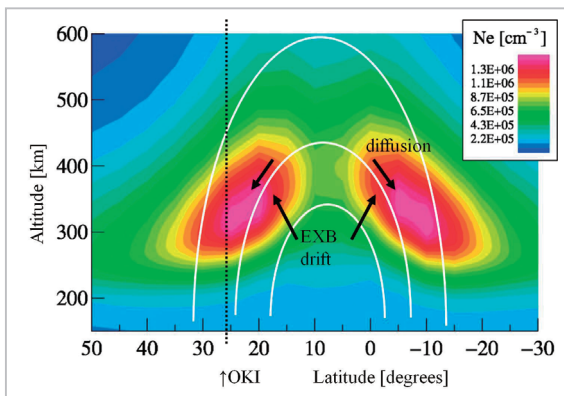


**Fig.2** Formation of the equatorial ionization anomaly (EIA)

A latitude-altitude distribution of the ionosphere during the daytime (at 12:00LT). The distribution of the ionosphere was obtained from the empirical international reference ionospheric model (IRI). The white curve represents the magnetic field lines of the earth. The black arrows show the movements of ionospheric plasma. The black vertical lines correspond to the latitudes (near Okinawa) shown in Fig. 1.

dynamo, Chapter 3 describes in detail the electrodynamics model incorporated in real-time ionosphere and thermosphere simulations conducted by NICT, and Chapter 4 presents several examples of calculations performed with the electrodynamics model, shows the relation between daily changes in the ionosphere at mid-latitudes and the ionospheric dynamo based on the simulations.

## 2 Generation of electric fields and currents due to the ionospheric dynamo

### 2.1 What is the ionospheric dynamo?

A dynamo generally refers to something that generates power. In the case of ‘ionospheric dynamo’, it means a mechanism that converts the kinetic energy of background thermospheric fluid moving against the ionospheric plasma into the electrostatic energy, whereby currents and electric fields are generated through the collision between the plasma and the neutral atmosphere. More specifically, the following two stages are often taken together when one refers to the ionospheric dynamo.

(1) When the thermospheric fluid moves against the ionospheric plasma with collisions between them in the presence of the Earth’s magnetic field, the drag force of the neutral atmosphere drives the drift motion of plasma. The resultant difference in the drift motion of ions and electrons causes a current to flow (‘dynamo current’).

(2) Since the electric conductivity is not spatially uniform in the ionosphere, the divergence and convergence of dynamo current cause electric charge to be accumulated. The resultant polarization electric field further drives the plasma drift. With collision with the neutral atmosphere, the drift motion is not unique between ions and electrons, thus resulting in a flow of current (‘polarization current’).

### 2.2 Ohm’s law in the ionosphere

The direction and magnitude of ion and

electron drifts (described in Section 2.1) change with altitude. Figure 3 shows the altitude variations in the ion and electron drifts driven by atmospheric drag and electric field (from Reference [3]). Since the density of neutral atmosphere quickly becomes smaller with altitude. At lower altitudes, both ions and electrons exhibit dominant motion due to collision with the neutral atmosphere. At higher altitudes, the drift motion ‘frozen-into’ the geomagnetic field becomes dominant. The altitude at which these effects switch over is much lower for electrons than for ions. For that reason, with respect to the drift due to atmospheric drag, it causes ions to be dragged

in the direction of motion  $\mathbf{u}_\perp$  ( $= \frac{\mathbf{B}}{B} \times \mathbf{u} \times \mathbf{B}$ ,

where  $\mathbf{u}$  denotes the neutral atmospheric velocity vector and  $\mathbf{B}$  the magnetic field vector) in the  $\mathbf{E}$  region. At higher altitudes, the ion drift begins to move in the direction of  $\mathbf{u} \times \mathbf{B}$ , while electrons remain trapped in the geomagnetic field, which results in the dynamo current flowing in the same direction as the ion drift. On the other hand, with respect to the drift driven by electric field, the ion drift changes from the direction  $\mathbf{E}_\perp$  (where  $\mathbf{E}$  denotes the electric field vector) to the direction  $\mathbf{E}_\perp \times \mathbf{B}$  toward the F region, while

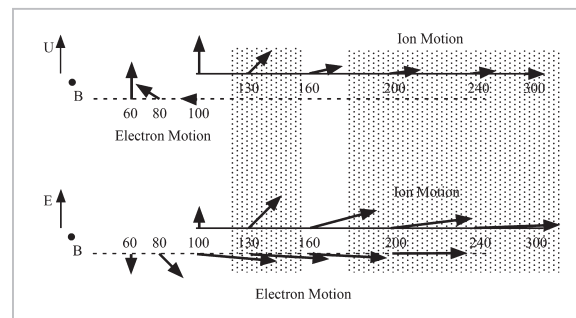


**Fig.3** Altitude dependence of ion and electron drifts due to atmospheric drag and electric field (from Reference [3])

The horizontal direction represents altitude. The rightward means higher altitude (with values denoting altitude). The ionospheric E and F regions are shaded separately. The drift direction is relative to geomagnetic field  $\mathbf{B}$  and neutral wind  $\mathbf{u}_\perp$  (electric field  $\mathbf{E}_\perp$ ) (not the rightward arrow indicating the upward drift).

the electron drift is in the direction  $\mathbf{E}_\perp \times \mathbf{B}$ . Therefore, the polarization currents flow in the direction  $\frac{\mathbf{B}}{B} \times \mathbf{E}_\perp$  (carried by electrons) and in the direction  $\mathbf{E}_\perp$  (carried by ions) in the E region, while current flowing in the direction  $\mathbf{E}_\perp$  remains in the F region. In the upper F region, both electrons and ions drift in the direction  $\mathbf{E}_\perp \times \mathbf{B}$ , and thus no polarization current flows transverse to the geomagnetic field.

The following numerical expressions summarize the currents generated in the ionospheric dynamo:

$$\begin{aligned} \mathbf{j}_\perp &= \sigma_p \mathbf{u} \times \mathbf{B} + \sigma_H \frac{\mathbf{B}}{B} \times \mathbf{u} \times \mathbf{B} + \sigma_p \mathbf{E}_\perp + \sigma_H \frac{\mathbf{B}}{B} \times \mathbf{E}_\perp \\ &= \sigma_p (\mathbf{E}_\perp + \mathbf{u} \times \mathbf{B}) + \sigma_H \frac{\mathbf{B}}{B} \times (\mathbf{E}_\perp + \mathbf{u} \times \mathbf{B}) \quad \dots (1 \text{ a}) \end{aligned}$$

$$\mathbf{j}_\parallel = \sigma_0 \mathbf{E}_\parallel \quad \dots (1 \text{ b})$$

$\mathbf{j}_\perp$  and  $\mathbf{j}_\parallel$  are the current vectors perpendicular and parallel components to the magnetic field lines, respectively. Here,  $\sigma_p$  and  $\sigma_H$  denote the electric conductivities of the ionosphere in directions perpendicular to the geomagnetic field (where Pedersen conductivity  $\sigma_p$  is the component in direction  $\mathbf{E}_\perp$ , and Hall conductivity  $\sigma_H$  in direction  $\hat{\mathbf{b}} \times \mathbf{E}_\perp$ ), while  $\sigma_0$  is the electric conductivity of the ionosphere in the direction along the magnetic field lines, expressed as follows;

$$\begin{aligned} \sigma_p &= \frac{n_e e}{B} \left( \frac{v_{in} \Omega_i}{v_{in}^2 + \Omega_i^2} + \frac{v_{en\perp} \Omega_e}{v_{en\perp}^2 + \Omega_e^2} \right) \\ \sigma_H &= \frac{n_e e}{B} \left( \frac{\Omega_e^2}{v_{en\perp}^2 + \Omega_e^2} - \frac{\Omega_i^2}{v_{in}^2 + \Omega_i^2} \right) \quad \dots (1 \text{ c}) \\ \sigma_0 &= \frac{n_e e^2}{m_e (v_{en\parallel} + v_{e\parallel})} \end{aligned}$$

where  $n_e$  denotes the electron density,  $e$  the elementary charge, and  $\Omega_i$  ( $\Omega_e$ ) and  $v_{in}$  ( $v_{en}$ ) the gyro frequency of the ions (electrons) and collision frequency with the neutral atmosphere, respectively. For the derivation of (Equation 1), see References [1] and [3]. On the first line of (Equation 1 (a)), the first and second terms on the right hand side are the dynamo currents due to the neutral atmospheric drag; the third and fourth terms denote

polarization currents due to polarization electric field. In the expression on the second line of (Equation 1 (a)),  $\mathbf{E}_\perp + \mathbf{u} \times \mathbf{B}$  can be considered as an electric field seen in the coordinate system that moves together with the neutral atmosphere. Therefore, (Equation 1) expresses Ohm's law connecting electric field to current.

### 2.3 Generation of the current system and electric field distribution in the ionosphere

This section describes how the ionospheric dynamo presented in the preceding section generates the ionospheric current system, and the east-west electric field at low altitude that induces EIA in the daytime F-region electron density distribution. Figure 4 (a) shows the global flow of the thermospheric atmosphere integrated over 100–300km at 0:00 in universal time (UT) in autumn equinox (September). This wind velocity field is obtained from an empirical model (HWM93 [4]) and, for the sake of simplicity, with only the diurnal component being extracted. Roughly speaking, one can see that the thermospheric fluid moves out in a radial direction from the region near the geographical equator in the afternoon sector, and that it converges to the region in the early morning sector at the geographical equator. Figure 4 (b) and (c) are the results of dynamo currents calculated by using (Equation 1 (a)) on the basis of those flows. Figure 4 (b) indicates the Pedersen current (corresponding to the first term on the RHS of the first line of Equation 1 (a)); Fig. 4 (c) indicates the Hall current (similarly corresponding to the second term). In the calculations of (Equation 1 (c)), the ion/electron density and temperature distributions were utilized from the International Reference Ionosphere (IRI) [5]. The density and temperature distributions of the neutral atmosphere were obtained from the empirical model of the upper neutral atmosphere (NRLMSIS) [6]. Since electric conductivity is large in the E region during the daytime, the dynamo current in Fig. 4 (b) and (c) also flows mostly during the daytime. As is evident from the figure, the ionospheric cur-

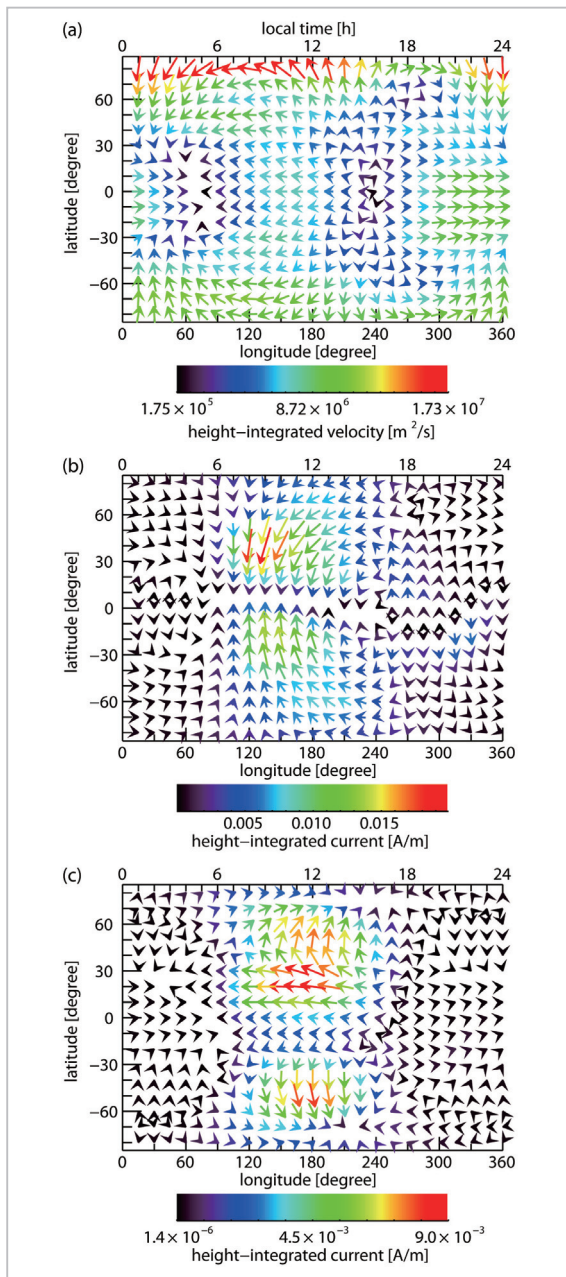


**Fig.4** Generation of dynamo current due to thermospheric neutral winds

(a) Wind velocity field in the thermosphere (September, 0:00 in UT, diurnal component), (b) Horizontal component of Pedersen dynamo current driven by the neutral winds in (a), and (c) Horizontal component of Hall dynamo current. The panels (a) to (c) are all integrated over altitudes from 100 to 300 km.

rent is not closed with the dynamo current alone. The discontinuity in the dynamo current causes charge accumulation, resulting in a polarization electric field. As later shown in Chapter 4, combining the dynamo and polar-

ization currents will generate a global closed current system in the ionosphere (called Sq current) that circulates throughout the low to mid latitudes in the daytime sector.

Figure 4 (b) shows an intense convergence of dynamo current to the sunrise sector at the magnetic equator. Here, positive charge is accumulated. In contrast, dynamo current diverges from around the sunset sector at the equator, with negative charge being accumulated. Therefore, an eastward polarization electric field is setup at low latitude during the daytime. This electric field induces polarization current in the E region, and at the same time it propagates to the F region along the geomagnetic field lines that can be regarded as equal-potential. This eastward electric field drives EIA in the F region as described in Chapter 1.

As stated above, the ionospheric dynamo with its origin in the background neutral atmospheric motion plays essential roles for the generation of EIA in the F region and the global ionospheric current system. On the other hand, atmospheric motion is not static in the thermosphere: it usually changes on various spatial and temporal scales, particularly due to gravity waves, atmospheric tides, and planetary waves. Many of those waves are originated in the atmospheric region below the thermosphere and propagated upwards. Therefore, these atmospheric waves cause significant changes in the ionospheric current system and the development of EIA through the ionospheric dynamo. Daily changes in the low-to-mid latitude ionosphere as presented in Chapter 1 also presumably occur due to the effects of atmospheric waves. Investigations of how and which atmospheric waves lead to day-to-day changes in the ionosphere thus pose an important challenge to be addressed in order to achieve numerical ionospheric forecasts. The simulation model for the electrodynamic process, such as presented in the next chapter, can be coupled with atmospheric and ionospheric models to offer an effective means of addressing this challenge.

In the above statement, we only refer to

'E-region dynamo' in which electric current flows mainly through the E region during the daytime, resulting in a polarization electric field. On the other hand, the electric conductivity of the E region declines at nighttime, so that current flowing in the F region becomes relatively large and generates polarization electric field. This is called the F region dynamo. Around the sunset, sudden changes occur from the E region to the F region dynamo. Although not treated in this paper, such sudden change causes a dynamic motion of F-region plasma around the sunset, which eventually leads to the generation of plasma bubbles (see Reference [7] and other parts of this special issue for details). The occurrence and development of plasma bubble is also considered to be affected by atmospheric waves via the ionospheric dynamo.

### 3 Numerical models expressing the ionospheric dynamo

Many researchers have developed numerical models expressing the ionospheric dynamo (ionospheric electrodynamics models). In early models where the ionosphere was assumed as being thin layer, the earth's current system was solved on a horizontal two-dimensional plane (see Reference [8]). The models capable of treating the earth's current system in three-dimensional space gradually became mainstream (see References [9] to [11]), and an electrodynamics model incorporating a realistic configuration of the earth's magnetic field emerged [12]. Moreover, it is now possible to incorporate an electrodynamics model as an element of regionally integrated model comprising the neutral atmospheric region and the ionospheric region [13]. This chapter introduces the technique employed in our ionospheric electrodynamics model (referred to as the HJEDYN model). This chapter also describes the model in detail, so that readers not interested in the simulation may skip it.

#### 3.1 Equations and coordinate system

Equations treated in the ionospheric elec-

trodynamic model include Ohm's law (Equation 1), the following equations for the current continuity (Equation 2) and for the assumption that we treat only electrostatic potential expressed as  $S$  (Equation 3).

$$\nabla(\mathbf{j}_{\perp} + \mathbf{j}_{\parallel}) = 0 \quad \dots (2)$$

$$\mathbf{E}_{\perp} = -\nabla_{\perp} S \quad \dots (3)$$

The selection of the appropriate coordinate system generally makes it easier to treat equations numerically. In the case of ionospheric dynamo, it is appropriate to use a coordinate system that matches the configuration of the Earth's magnetic field. In the low to mid latitude regions, at altitudes where most current flows (higher than 90 km), the relation  $\sigma_0 \gg \sigma_P, \sigma_H$  holds true. Thus, when a charge separation generates along the geomagnetic field lines, a very weak electric field will readily cause a current to flow so as to reduce the charge separation. Consequently, the geomagnetic field lines can be regarded as equipotential, so that if one coordinate variable is chosen in the direction of the magnetic field lines, then the number of dimensions will be reduced by one, thereby making it easier to solve the equations as shown later on. In the HJEDYN model, the apex coordinates are used similar to Reference [12]. Figure 5 shows

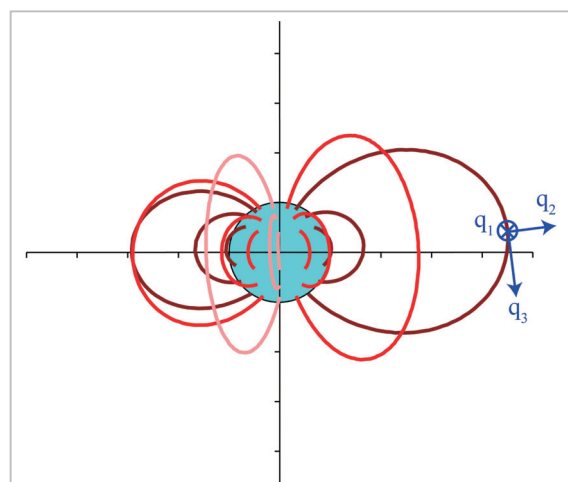


**Fig.5** The earth's magnetic field lines and the coordinate system of the electrodynamics model

the coordinate system. Note that  $q_1$  in the figure is  $\phi_a$  (magnetic longitude of the apex of the magnetic field lines),  $q_2$  is  $\lambda_a$  (magnetic latitude of the point where the magnetic field lines intersect the ground surface (here we take northern portion)),  $q_3$  is  $V_B/(r_0B_0)$  (indicating location along the magnetic field lines, where  $V_B$  denotes the magnetic potential ( $\mathbf{B} = -\nabla V_B$ ) and  $B_0$  the intensity of the main magnetic field of the dipole component)). (Equation 1) to (Equation 3) are developed on the above-mentioned coordinate system. Since direction  $q_1$  and direction  $q_2$  are not mutually orthogonal, two sets of basis vectors are necessary. The base vectors are defined as follows:

$$\begin{aligned} \mathbf{d}_i &= \nabla q_i \\ \mathbf{e}_i &= \frac{\partial \mathbf{r}}{\partial q_i} \end{aligned} \quad \dots (4)$$

And their mutual relation is set as follows:

$$\begin{aligned} \mathbf{d}_i \cdot \mathbf{e}_j &= \delta_{ij} \\ \mathbf{e}_i &= W \mathbf{d}_j \times \mathbf{d}_k \\ \mathbf{d}_i &= \frac{1}{W} \mathbf{e}_j \times \mathbf{e}_k \\ W &= \mathbf{e}_i \cdot \mathbf{e}_j \times \mathbf{e}_k = (\mathbf{d}_i \cdot \mathbf{d}_j \times \mathbf{d}_k)^{-1} \end{aligned} \quad \dots (5)$$

These equations can be used to develop Ohm's law (Equation 1) as in the following equation:

$$\begin{aligned} \mathbf{j}_\perp &= j_{e1} \mathbf{e}_1 + j_{e2} \mathbf{e}_2 \\ j_{e1} &= (E_{d1} + u_{e2} B_{e3} W) \sigma_p d_1^2 \\ &\quad + (E_{d2} - u_{e1} B_{e3} W) \left( \sigma_p \mathbf{d}_1 \cdot \mathbf{d}_2 + \frac{B_0 \sigma_H r_0}{BW} \right) \\ j_{e2} &= (E_{d1} + u_{e2} B_{e3} W) \left( \sigma_p \mathbf{d}_1 \cdot \mathbf{d}_2 - \frac{B_0 \sigma_H r_0}{BW} \right) \\ &\quad + (E_{d2} - u_{e1} B_{e3} W) \sigma_p d_2^2 \end{aligned} \quad \dots (1')$$

Since it is assumed that the magnetic field lines are equipotential, the direction along the magnetic field lines (Equation 1 (b)) is therefore not used here. The equation for the current continuity (Equation 2) is as in the following equation:

$$\begin{aligned} \frac{1}{W} \frac{\partial}{\partial q_1} (\mathbf{e}_2 \times \mathbf{e}_3 \cdot \mathbf{j}_\perp) + \frac{1}{W} \frac{\partial}{\partial q_2} (\mathbf{e}_3 \times \mathbf{e}_1 \cdot \mathbf{j}_\perp) &= -\frac{1}{W} \frac{\partial}{\partial q_3} (\mathbf{e}_1 \times \mathbf{e}_2 \cdot \mathbf{j}_\perp) \\ \rightarrow \frac{\partial}{\partial q_1} (W j_{e1}) + \frac{\partial}{\partial q_2} (W j_{e2}) &= -\frac{\partial}{\partial q_3} (W j_{e3}) \end{aligned} \quad \dots (2')$$

The assumption of treating electrostatic elec-

tric field (Equation 3) can be expressed in the following equation:

$$\mathbf{E} = E_{d1} \mathbf{d}_1 + E_{d2} \mathbf{d}_2 = -\frac{\partial S}{\partial q_1} \mathbf{d}_1 - \frac{\partial S}{\partial q_2} \mathbf{d}_2 \quad \dots (3')$$

Summarizing (Equation 1') to (Equation 3') in terms of electrostatic potential and integrating along the magnetic field lines will produce the following equation:

$$\begin{aligned} \frac{\partial}{\partial q_1} \left( \Sigma_{11} \frac{\partial S}{\partial q_1} + (\Sigma_{12} + \Sigma_H) \frac{\partial S}{\partial q_2} \right) + \frac{\partial}{\partial q_2} \left( (\Sigma_{12} - \Sigma_H) \frac{\partial S}{\partial q_1} + \Sigma_{22} \frac{\partial S}{\partial q_2} \right) \\ - \frac{\partial K_1}{\partial q_1} - \frac{\partial K_2}{\partial q_2} = W [j_{e3}]_{q_3^a}^{q_3^b} \end{aligned} \quad \dots (6)$$

Each factor on the left hand side of (Equation 6) is an integral value along the following magnetic field lines;

$$\begin{aligned} \Sigma_{11} &= \int_{q_3^a}^{q_3^b} \sigma_p \frac{d_1^2}{|\mathbf{d}_1 \times \mathbf{d}_2|} \frac{dq_3}{d_3} & \Sigma_{12} &= \int_{q_3^a}^{q_3^b} \sigma_p \frac{\mathbf{d}_1 \cdot \mathbf{d}_2}{|\mathbf{d}_1 \times \mathbf{d}_2|} ds \\ \Sigma_{22} &= \int_{q_3^a}^{q_3^b} \sigma_p \frac{d_2^2}{|\mathbf{d}_1 \times \mathbf{d}_2|} \frac{dq_3}{d_3} & \Sigma_H &= \int_{q_3^a}^{q_3^b} \sigma_H \frac{dq_3}{d_3} \\ K_1 &= \int_{q_3^a}^{q_3^b} B_{e3} W \left[ \sigma_p u_{e2} \frac{d_1^2}{|\mathbf{d}_1 \times \mathbf{d}_2|} - \left( \sigma_H + \sigma_p \frac{\mathbf{d}_1 \cdot \mathbf{d}_2}{|\mathbf{d}_1 \times \mathbf{d}_2|} \right) u_{e1} \right] \frac{dq_3}{d_3} \\ K_2 &= \int_{q_3^a}^{q_3^b} B_{e3} W \left[ \left( \sigma_p \frac{\mathbf{d}_1 \cdot \mathbf{d}_2}{|\mathbf{d}_1 \times \mathbf{d}_2|} - \sigma_H \right) u_{e2} - \sigma_p u_{e1} \frac{d_2^2}{|\mathbf{d}_1 \times \mathbf{d}_2|} \right] \frac{dq_3}{d_3} \end{aligned} \quad \dots (7)$$

where  $q_3^a$  and  $q_3^b$  denote the start and end points of integration along the magnetic field lines, respectively. If the range of integration is set sufficiently large so that the start and end are taken at the bottom of the ionosphere in the Northern and Southern Hemispheres, the current vanishes to 0 and expressed as follows:

$$W [j_{e3}]_{q_3^a}^{q_3^b} = 0 \quad \dots (8)$$

Therefore, under (Equation 8), (Equation 6) becomes a two-dimensional partial differential equation concerning  $S(q_1, q_2)$ .

In order to accurately determine the electric fields and currents in the ionosphere under the realistic configuration of geomagnetic field, one must properly treat the set of base vectors  $\mathbf{d}_i$  and  $\mathbf{e}_i$  and (Equation 7) as stated above. With respect to the actual configuration of geomagnetic field, the International Geomagnetic Reference Field (IGRF) model can be used (<http://www.ngdc.noaa.gov/IAGA/>

vmod/igrf.html). Simplifying the geomagnetic field configuration to be a dipole magnetic field will considerably make easier the calculations. In that case, the directions of base vectors  $\mathbf{d}_i$  and  $\mathbf{e}_i$  are identical, and base vectors of the same kind are mutually orthogonal ( $\mathbf{d}_i \cdot \mathbf{d}_j = \mathbf{0}, i \neq j$ ) and further can be expressed by using polar coordinate variables ( $r, \theta, \varphi$ ) that make it easier to calculate integral values along the magnetic field lines (Equation 7) (such as Reference [9]).

### 3.2 Numerical techniques

When neutral atmospheric wind velocity and electric conductivity are given globally, the integral values along the magnetic field lines from (Equation 7) can be calculated. Then, (Equation 6) can be numerically solved under the appropriate boundary conditions. Many researchers have developed numerical models that treat the ionospheric dynamo, most of them basically treating the similar equation (Equation 6). In the following, the numerical treatment of the HJEDYN model is introduced below. The HJEDYN model has been developed so that it would become an element of whole atmosphere-ionosphere coupled model (together with an ionospheric model [14] and a whole atmospheric general circulation model (GCM) [15][16]), and incorporated into a real-time simulation [17] for space weather forecasts. For that reason, the model has been developed in consideration of (i) robustness (so calculations always converge in a stable manner), (ii) high calculation speed, and (iii) high spatial resolution (save memory at the same time).

In the HJEDYN model, the equations are differentiated by using a finite volume technique because it can be well fit to the boundary conditions. Thus, (Equation 6) is changed as follows:

$$\begin{aligned} \frac{\partial J_1}{\partial q_1} + \frac{\partial J_2}{\partial q_2} &= 0 \\ J_1 &= -\Sigma_{11} \frac{\partial S}{\partial q_1} - (\Sigma_{12} + \Sigma_H) \frac{\partial S}{\partial q_2} + K_1 \\ J_2 &= -(\Sigma_{12} - \Sigma_H) \frac{\partial S}{\partial q_1} - \Sigma_{22} \frac{\partial S}{\partial q_2} + K_2 \end{aligned} \quad \dots (6')$$

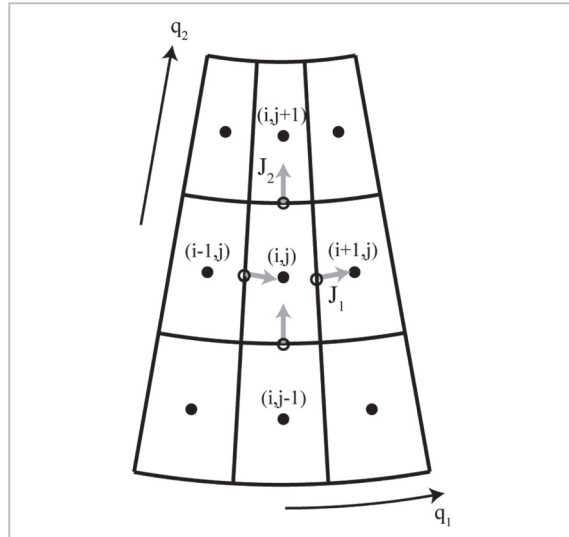


**Fig.6** Distribution of grid points and currents in the electrodynamic model

The distribution of grid points and currents (integral quantities  $J_1, J_2$ ) in a two-dimensional ( $q_1, q_2$ ) calculation space in the electrodynamic model. The black circles represent the center of each grid where the quantities such as electrostatic potential are placed. The white circles represent inter-grid boundaries where the currents are placed.

$J_1$  and  $J_2$  are the  $q_1$  and  $q_2$  components of current integrated along the magnetic field lines (when multiplied by an area element), respectively. Figure 6 shows the distributions of grid point and physical quantities in a two-dimensional space consisting of  $q_1$  and  $q_2$ . The grid numbers are set as  $i = 1, 2, \dots, imax$  in the direction of  $q_1$ , and as  $j = 1, 2, \dots, jmax$  in the direction of  $q_2$ . As shown in Fig. 6, the electrostatic potential  $S$  is defined at the grid center  $(i, j)$  and the currents  $J_1$  and  $J_2$  are defined at the inter-grid boundaries  $(i \pm 1/2, j)$  and  $(i, j \pm 1/2)$ . The current of (Equation 6') is expressed with a differential equation as follows:

$$\begin{aligned} J_1(i + 1/2, j) &= -\left[ \frac{5}{6} \Sigma_{11}(i + 1/2, j) \frac{S(i+1, j) - S(i, j)}{\Delta q_1} \right. \\ &+ \frac{1}{12} \Sigma_{11}(i + 1/2, j-1) \frac{S(i+1, j-1) - S(i, j-1)}{\Delta q_1} \\ &+ \left. \frac{1}{12} \Sigma_{11}(i + 1/2, j+1) \frac{S(i+1, j+1) - S(i, j+1)}{\Delta q_1} \right] \\ &- \left[ \Sigma_{12}(i + 1/2, j) + \Sigma_H(i + 1/2, j) \right] \frac{S(i, j+1) - S(i, j-1)}{2\Delta q_2} + K_1(i + 1/2, j) \end{aligned} \quad \dots (9 a)$$

$$\begin{aligned}
J_2(i, j + 1/2) = & -[\Sigma_{12}(i, j + 1/2) - \Sigma_{11}(i, j + 1/2)] \frac{S(i+1, j) - S(i-1, j)}{2\Delta q_1} \\
& - \left[ \frac{5}{6} \Sigma_{22}(i, j + 1/2) \frac{S(i, j+1) - S(i, j)}{\Delta q_2} \right. \\
& + \frac{1}{12} \Sigma_{22}(i-1, j + 1/2) \frac{S(i-1, j+1) - S(i-1, j)}{\Delta q_2} \\
& \left. + \frac{1}{12} \Sigma_{22}(i+1, j + 1/2) \frac{S(i+1, j+1) - S(i+1, j)}{\Delta q_2} \right] + K_2(i, j + 1/2) \quad \dots (9 \text{ b})
\end{aligned}$$

In the differential term in the  $J_1$  equation in the direction of  $q_1$  and in the term in the  $J_2$  equation in the direction of  $q_2$ , the contribution of the difference between the neighboring grids with a certain fraction is added in order to reduce the truncation error due to the difference between the second-order differentiation terms. In grids other than the boundaries, the following equation that differentiates the first line of (Equation 6') is applied:

$$\frac{J_1(i + 1/2, j) - J_1(i - 1/2, j)}{\Delta q_1} + \frac{J_2(i, j + 1/2) - J_2(i, j - 1/2)}{\Delta q_2} = 0 \quad \dots (10)$$

The boundary conditions in the direction of  $q_1$  ( $\phi_a$ : apex longitude) are periodic boundaries, that is:

$$J_1(i_{\max} + 1/2, j) = J_1(1/2, j) \quad \text{for all } j \quad \dots (11 \text{ a})$$

So as to satisfy the current closure at the bottom of the ionosphere, the boundary condition at  $j = 1$  in the direction of  $q_2$  ( $\lambda_a$ : magnetic latitude at the intersection of the magnetic field lines with the ground surface) is;

$$J_2(i, 1/2) = 0 \quad \text{for all } i \quad \dots (11 \text{ b})$$

together with  $S(i, 0) = S(i, 1)$ . At  $j = j_{\max}$ ,

$$\sum_i J_2(i, j_{\max} + 1/2) = 0 \quad \dots (11 \text{ c})$$

was set in order to ensure that the currents flowing into and out from the magnetic poles are balanced. The electrostatic potential of the poles was also selected as the reference point and  $S(i, j_{\max} + 1) = 0$  was set. The ionospheric currents should be connected to the magnetospheric currents at the high-latitude region, which remains a challenge to be addressed in the future. (Equation 6) is sensitive to the boundary setting and the treatment of bound-

aries is important to ensure robustness. Defining the current at the inter-grid boundaries as in (Equation 9) will facilitate the treatment of boundary conditions as in (Equation 11 (a)) to (Equation 11 (c)). Concerning robustness, it is important to reduce the truncation error in the difference equation (Equation 9).

The index  $[i, j]$  is put together to express as  $m = i_{\max} \times (j - 1) + i$ . Then, substituting (Equation 9) into (Equation 10) will produce a dynamo difference equation using an index  $m$ .

$$\begin{aligned}
& a(m, m - i_{\max} - 1) S(m - i_{\max} - 1) \\
& + a(m, m - i_{\max}) S(m - i_{\max}) \\
& + a(m, m - i_{\max} + 1) S(m - i_{\max} + 1) \\
& + a(m, m - 1) S(m - 1) + a(m, m) S(m) \\
& + a(m, m + 1) S(m + 1) \\
& + a(m, m + i_{\max} - 1) S(m + i_{\max} - 1) \\
& + a(m, m + i_{\max}) S(m + i_{\max}) \\
& + a(m, m + i_{\max} + 1) S(m + i_{\max} + 1) \\
& = b(m) \quad \dots (12)
\end{aligned}$$

Here,  $a(m, n)$  and  $b(m)$  are coefficients expressed by using the integral quantity along the magnetic field lines from (Equation 7). For the boundary conditions in (Equation 11 (a)) to (Equation 11 (c)), substituting (Equation 9) into them will make it a linear equation with respect to electrostatic potential  $S$ . Therefore, the equation can be transformed into the following linear equation;

$$\sum_{n=1}^{m_{\max}} a(m, n) S(n) = b(m) \quad \dots (13)$$

Indexes  $m$  and  $n$  each take a range from 1 to  $m_{\max}$  ( $m_{\max} = i_{\max} \times j_{\max}$ ). (Equation 13) can be solved numerically by using general appropriate methods. After distribution of electrostatic potential is solved, the distributions of electric fields and currents can be derived by (Equation 1'), (Equation 3') and (Equation 6).

## 4 Reproduction of the ionospheric dynamo with the electro-dynamics model

This chapter presents some examples of calculations using the electro-dynamics model described in Chapter 3. Figure 7 compares the

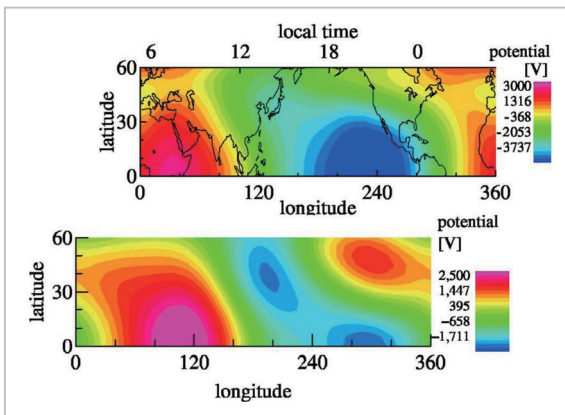


**Fig.7** Comparison between electrostatic potential reproduced by the electrodynamics model (top panel) and an empirical model [19] (bottom panel).

Because the universal times (UT) compared are different, the two figures are shifted in longitude direction to match the local time (LT).

distribution of electrostatic potential calculated using the HJEDYN model with an empirical model [19]. In the calculation, we used as the input distributions of electric conductivity and neutral atmospheric wind velocity, the International Reference Ionosphere (IRI) [5] and the extended atmospheric general circulation model [15][16]. Although the considered season is the same (September), the HJEDYN model treats a medium degree of solar activity ( $F_{10.7} = 135$ ), while the empirical model treats low solar activity, which may lead to the difference in the range of global potential variation. The overall potential distribution at low to mid latitudes is similar between both the models, indicating that the ionospheric dynamo contributes mainly to the formation of observed potential distribution.

Figure 8 shows the current distribution reproduced by the HJEDYN model with black arrows and displays the electrostatic potential with contours. The current is a value integrated along the magnetic field lines and projected onto the point where the magnetic field lines intersect the altitude of 70 km in the Northern Hemisphere. (The calculations in Fig. 7 only

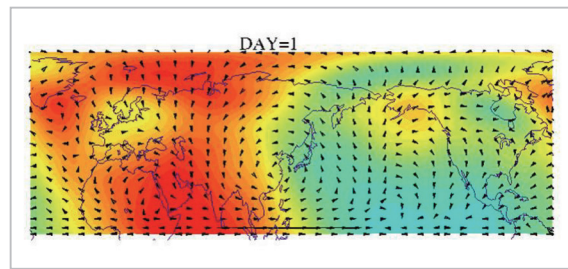


**Fig.8** Current distribution and electrostatic potential reproduced by the electrodynamics model

The current distribution (arrow) and electrostatic potential (contours) reproduced by the electrodynamics model. The currents are integrated along the magnetic field lines and projected onto the plane where the magnetic field lines intersect an altitude of 70 km.

used the diurnal and semidiurnal migrating tidal winds as input from the atmospheric general circulation model, while the calculation in Fig. 8 used all tidal components.) As shown in Fig. 8, the low to mid-latitude regions during the daytime constitute one larger eddy current. As described in Section 2.3, the dynamo current driven directly by the neutral atmospheric motion is discontinuous, but the polarization current fills to meet the current continuity in the entire region. The simulation also reproduces an intensified eastward current at the magnetic equator during the daytime, i.e., the equatorial electrojet current (EEJ) (see [20] in this special issue). In addition to a large Sq current system during daytime, small eddy current structures are seen around the sunset and sunrise at low latitudes, adding complexities to the ionospheric current distribution. These structures are not constant and exhibit highly temporal variations. Such fine structures and temporal variations stem from the wind velocity distribution from the atmospheric general circulation model and its temporal changes. Although verification through comparison with observations is necessary, such variations are quite interesting in terms of the relation with the ionospheric day-to-day variations.

Chapter 1 described how fluid waves in the thermosphere modulated the east-west

electric field at low altitudes through the dynamo process and change the latitudinal growth of EIA. Future prediction of the electron density variation in the ionosphere at mid-latitudes requires the reproduction of these processes with simulation models. As a feasible study, a series of neutral wind distributions during the 30 days of September obtained from an atmospheric global circulation model was used as input into the HJE-DYN model, and the 30-day variation in the electric field distribution was calculated. Moreover, the distributions of electric field and neutral wind were utilized as input into another ionospheric model (SAMI2)[21], and daily change in the ionospheric density distribution was calculated. Figure 9 (a) and (b)

show part of the results. Figure 9 (a) is a five-day variation of F-region electron density distribution at the low-to-middle latitudes. There are separate regions of high density across the magnetic equator (EIA), and the growth of EIA in latitude varies on the day-to-day basis.

The top panel in Fig. 9 (b) is a 20-day variation of electron density at mid-latitude reproduced by the same simulation. This figure displays NmF2 at 27° N geographic latitude. From the figure, one can see how NmF2 changes daily. For example, from September 27 to 28, the NmF2 maximum during the daytime almost doubled. This is due to the expansion of EIA to the high-latitude as shown in Fig. 9 (a). Chapter 1 explained the relation between the EIA growth and the electric field generated in the dynamo process. The bottom panel in Fig. 9 (b) displays the east-west electric field at the magnetic equator and at an altitude of 300 km. A comparison with NmF2 in the top panel of Fig. 9 (b) indicates a good correlation between the intensity of the eastward electric field and NmF2 during the daytime. For example, September 18, 20, 24 and 27 experienced smaller eastward electric fields during the daytime than on the previous or following days, and NmF2 at mid-latitude was also smaller. However, there were some days (such as around September 14) when the correlation was not so good between the equatorial electric field and mid-latitude NmF2. This is because the ionospheric density is not affected only by the growth of EIA due to electric fields but also by changes in the neutral composition of the background thermosphere and meridional wind velocity along the magnetic field lines.

Figure 9 (c) is a five-day (September 24–28, 2006) variation of NmF2 observed by the ionosonde at Okinawa (26.68° N geographic latitude). We selected the same month as that of the simulation shown in Fig. 9 (a) and (b) under the condition of low solar activity and low geomagnetic turbulence. Figure 9 (c) shows variations with a period of two to three days in addition to shorter-scale temporal changes with a period of several hours, and

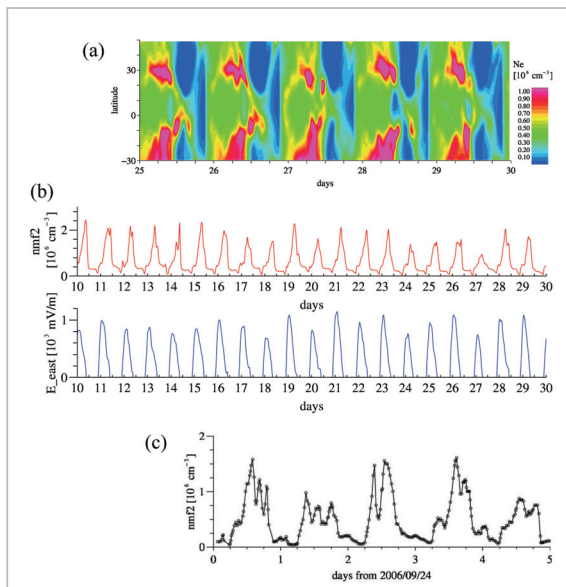


**Fig. 9** Comparison of the ionospheric density variations calculated based on the electric field obtained from the electrodynamics model with NmF2 at Okinawa

(a), (b): Results from ionospheric simulation using the input electric field variations from the electromagnetic model; (a) represents the temporal change in the electron density at an altitude of 300 km and at the longitude of Japan (at 135° E geographic longitude). (b) represents simulated NmF2 (F layer maximum electron density) at 27° N and the east-west electric field at 300 km height at the magnetic equator.  
(c) NmF2 observed by the ionosonde at Okinawa (26.68° N) on September 24–28, 2006

there are even some days when the NmF2 maximum is about double that of the preceding day. Similar daily variations are also reproduced by the simulation as shown in Fig. 9 (b), and the variations over a period of two to three days are reproduced both in mid-latitude NmF2 and the equatorial electric field. Therefore, the origin of daily variations in NmF2 as observed in Fig. 9 (c) may be considerably from the variations in the low-latitude ionospheric dynamo, as interpreted based on the simulation results, and the variations in the ionospheric dynamo originate in the various atmospheric waves propagating from low altitudes.

## 5 Conclusion

As presented in this paper, the ionospheric dynamo plays a significant role in connecting the background atmospheric motion and the ionospheric density variation through the generation of electric fields. Day-to-day changes in the ionosphere presumably originate in activities in the lower atmosphere that excite atmospheric waves. Therefore, this is the subject that regional coupled simulations work. In recent years, we have coupled the electrodynamics model introduced in this paper with an extended atmospheric model extending from

the ground surface to the upper thermosphere [15][16] and with an ionospheric model [14], thereby developing a model covering the entire atmospheric region of the earth. This whole atmosphere-ionosphere coupled model includes a series of physical processes described in this paper and will hopefully reproduce daily changes in the ionosphere on a quantitative basis. The calculations given in Chapter 4 show such example. However, reproducing and predicting ionospheric changes that match the actual ionospheric behaviors necessitate the incorporation of observational data into the model. Therefore, such technique for that purpose must be taken into account for the future development of the whole atmosphere-ionosphere model.

## Acknowledgments

This study used the calculation results of the extended atmospheric general circulation model developed at Kyushu University and Tohoku University. We also used ionospheric model SAMI2 developed at the United States Naval Research Laboratory. The World Data Center for Geomagnetism at Kyoto University provided the Kp indices of geomagnetic disturbances. We would like to express our deep appreciation and thanks to those institutions.

## References

- 1 Richmond, A. D., "Ionospheric Electrodynamics" in "Handbook of Atmospheric Electrodynamics", edited by H. Volland, CRC Press, Chapter 9, pp. 249–290, 1995.
- 2 Jin, H. and E. Sagawa, "Ionospheric Wavenumber 4 Longitudinal Structure," Special issue of this NICT Journal, 3–4–1, 2009.
- 3 Heelis R. A., "Electrodynamics in the low and middle latitude ionosphere: a tutorial," J. Atmos. Sol. Terr. Phys., Vol. 66, pp. 825–838, 2004.
- 4 Hedin, A. E. et al., "Empirical wind model for the upper, middle and lower atmosphere," J. Atmos. Terr. Phys., Vol. 58, pp. 1421–1447, 1996.
- 5 Bilitza, D., "International reference ionosphere 2000: Examples of improvements and new Features," Adv. Space Res., Vol. 31, pp. 757–767, 2003.
- 6 Picone, J. M., A. E. Hedin, D. P. Drob, and A. C. Aikin, "NRLMSISE-00 empirical model of the atmosphere: Statistical comparisons and scientific issues," J. Geophys. Res., Vol. 107, 1468, doi: 10.1029/2002JA009430, 2002.

- 7 T. Maruyama, S. Saito, M. Kawamura, K. Nozaki, J. Uemoto, T. Tsugawa, H. Jin, M. Ishii, and M. Kubota, "Outline of the SEALION Project and initial results," Special issue of this NICT Journal, 3–2–1, 2009.
- 8 Tarpley, J. D., "The ionospheric wind dynamo, áU, solar tides," Planetary and Space Science, Vol. 18, pp. 1091–1103, 1970.
- 9 Takeda, M. and H. Maeda, "Three-dimensional structure of ionospheric currents, 1, currents caused by diurnal tidal winds," Journal of Geophysical Research Vol. 85, pp. 6895–6899, 1980.
- 10 Kawano, K. S. and S. Miyahara, "A study on three-dimensional structures of the ionospheric dynamo currents induced by the neutral winds simulated by the Kyushu-GCM," J. Atmos. Sol. Terr. Phys. Vol. 70, pp. 1549–1562, 2008.
- 11 Jin, H., Y. Miyoshi, H. Fujiwara, and H. Shinagawa, "Electrodynamics of the formation of ionospheric wave number 4 longitudinal structure," J. Geophys. Res., Vol. 113, A09307, doi: 16510.1029/2008JA013301, 2008.
- 12 Richmond, A. D., "Ionospheric Electrodynamics Using Magnetic Apex Coordinates," J. Geomag. Geoelec., Vol. 47, pp. 191–212, 1995.
- 13 Richmond, A. D., E. C. Ridley, and R. G. Roble, "A thermosphere/ionosphere general circulation model with coupled electrodynamics," Geophys. Res. Lett., Vol. 19, pp. 601–604, 1992.
- 14 Shinagawa, H. and S. Oyama, "A two-dimensional simulation of thermospheric vertical winds in the vicinity of an auroral arc," Earth Planets Space, Vol. 58, pp. 1173–1181, 2006.
- 15 Miyoshi, Y. and H. Fujiwara, "Day-to-day variations of migrating diurnal tide simulated by a GCM from the ground surface to the exobase," Geophys. Res. Lett., Vol. 30, 1789, doi: 10.1029/2003GL017695, 2003.
- 16 Fujiwara, H. and Y. Miyoshi, "Characteristics of the large-scale traveling atmospheric disturbances during geomagnetically quiet and disturbed periods simulated by a whole atmosphere general circulation model," Geophys. Res. Lett., Vol. 33, L20108, doi: 10.1029/2006GL027103, 2006.
- 17 Shinagawa, H., "Ionosphere Simulation," Special issue of this NICT Journal, 2–3–6, 2009.
- 18 Barrett, R., M. Berry, T. F. Chan, J. Demmel, J. Donato, J. Dongarra, V. Eijkhout, R. Pozo, C. Romine, and H. van der Vorst, "Templates for the Solution of Linear Systems: Building Blocks for Iterative Methods," Society for Industrial Mathematics, 1987.
- 19 Richmond, A. D., M. Blanc, B. A. Emery, R. H. Wand, B. G. Fejer, R. F. Woodman, S. Ganguly, P. Amayenc, R. A. Behnke, C. Calderon, and J. V. Evans, "An Empirical Model of Quiet-Day Ionospheric Electric Fields at Middle and Low Latitudes," J. Geophys. Res. Vol. 85, p. 4658, 1980.
- 20 Uemoto, J., T. Maruyama, S. Saito, M. Ishii, and R. Yoshimura, "Relationship between equatorial electrojet variation and spread-F occurrence," Special issue of this NICT Journal, 3–2–4, 2009.
- 21 Huba, J. D., G. Joyce, and J. A. Fedder, "Sami2 is another model of the ionosphere (SAMI2): A new low-latitude ionosphere model," J. Geophys. Res., Vol. 105, pp. 23,035–23,053, 2000.



**JIN Hidekatsu, Dr. Sci.**

*Expert Researcher, Space Environment  
Group, Applied Electromagnetic  
Research Center  
Upper Atmospheric Physics*